

Article

Finite Element Study of Hyperstructure Systems with Modular Light-Frame Construction in High-Rise Buildings

Nicolas Labrecque ^{1,*} , Sylvain Ménard ², Marc Oudjene ³ and Pierre Blanchet ¹ 

¹ Department of Wood and Forest Sciences, Laval University, Quebec, QC G1V 0A6, Canada; pierre.blanchet@sbf.ulaval.ca

² Department of Applied Sciences, University of Quebec at Chicoutimi (UQAC), Saguenay, QC G7H 2B1, Canada; sylvain.menard@uqac.ca

³ Department of Civil and Water Engineering, Laval University, Quebec, QC G1V 0A6, Canada; marc.oudjene@gci.ulaval.ca

* Correspondence: nicolas.labrecque.2@ulaval.ca

Abstract: To answer both the growth of the world's urban population and the climate changes, new structural systems with high prefabrication levels and renewable materials need to be developed. A novel structural system that could enable the use of modular light-frame construction in high-rise buildings was modeled and analyzed. This system was achieved by having a hyperstructure carrying the loads of four-story light-frame superposed substructures. Two 20-story hyperstructures, one using glulam and another one using reinforced concrete, were designed according to the 2015 National Building Code of Canada and compared. A simplified model for the light-frame modules according to the CSA O86-19 was proposed. The interaction between both systems and the impact on the substructures were analyzed. The results of the response spectrum analysis and dynamic wind analysis show that, with a glulam hyperstructure, modules could be connected to the columns and the floors or only to the floors. With a concrete hyperstructure, the modules must be connected to the columns and the cores. For both systems, the design of shearwalls on the short side of the modules is governed by the lateral deformation imposed by seismic forces, while the design of shearwalls on the long side of the modules is governed by the vertical deformation of the primary beams under gravity loads. Standard shearwall assemblies are sufficient to resist the shear induced by gravitational, wind and seismic loads. The analysis indicates that the system could be viable, but more research should be especially performed on the connections between the substructures and the hyperstructure.

Keywords: hybrid structures; modular construction; light-frame substructures; innovative structural system; finite element analysis; wood construction



Citation: Labrecque, N.; Ménard, S.; Oudjene, M.; Blanchet, P. Finite Element Study of Hyperstructure Systems with Modular Light-Frame Construction in High-Rise Buildings. *Buildings* **2022**, *12*, 330. <https://doi.org/10.3390/buildings12030330>

Academic Editor: Alessandro Cannavale

Received: 28 January 2022

Accepted: 7 March 2022

Published: 9 March 2022

Publisher's Note: MDPI stays neutral with regard to jurisdictional claims in published maps and institutional affiliations.



Copyright: © 2022 by the authors. Licensee MDPI, Basel, Switzerland. This article is an open access article distributed under the terms and conditions of the Creative Commons Attribution (CC BY) license (<https://creativecommons.org/licenses/by/4.0/>).

1. Introduction

In 2050, the urban population is expected to be close to 7 billion, an increase of 50% compared to the actual situation [1]. To accommodate more than 2 billion new people without increasing too much urban sprawl and its environmental consequences, the densification of cities is mandatory [2]. In compact cities, the buildings, having higher volume-to-surface ratios, are more energy efficient [3]. Constructing in cities poses its challenges. Space for the construction site is very limited, neighbors are close and can be bothered by the noise and dust, and arteries closure can have increased consequences the longer the construction lasts for locality and nearby businesses [4]. The construction of tall buildings in cities must therefore be accelerated, less disruptive and less costly with prefabrication [5]. Light-frame modular construction allows for a high level of prefabrication. Insulation, mechanic and electric elements; cladding; doors and windows; wall and floor finishes; and even furniture and appliances can be installed in factories, diminishing the work to be performed onsite.

In the province of Quebec, Canada, and throughout North America, light-frame construction is limited at six stories by construction codes due to resistance and serviceability

limitations. Systems designed to receive internal substructures and to act as the main gravity and lateral load resisting system (LLRS) could enable the use of light-frame construction in high-rise buildings and need to be more explored so that the benefits of prefabrication can be further exploited [6].

Such design was explored with the building Treet, completed in Bergen, Norway, in 2015. Treet was the world's tallest timber building in 2015, and its innovative structural system was studied by many authors [7–10]. A similar structural system, but with the main structure made of concrete, was studied in recent years [6,11–13]. This structural concept is named FaB and was first proposed by Xiong et al. in 2016 [14]. Many numerical studies were also performed on innovative structural systems for high-rise timber buildings [3,9,15–18]. The studied systems were part of research concepts, but also real buildings, such as Mjøstårnet and Brock Commons. In the last decade, high-rise buildings using different modular structural systems were also constructed around the world [19–22].

Several numerical studies dealing with light wood-frame structures have been presented by many authors [23–29]. Models developed vary in regard to numerical complexity and precision compared to the tested structures and elements considered (walls, diaphragms, full house, etc.) [30–33]. Some researchers model light-frame behavior through shell elements, while others model it with linear elements, springs or a mix of the three latter. An interesting approach was suggested by Chen et al. [23], who worked on a pinned frame with diagonal members and vertical connectors.

The main aim of this study was to design a hyperstructure system that achieves the structural performance required for the use of modular light-frame in high-rise buildings. To achieve this, two different 20-story hyperstructure systems were designed, a method to model modular light-frame construction, using finite elements, was developed, and the interaction between both systems and the impact on the substructures were analyzed.

2. Materials and Methods

The structural concept to enable the use of light-frame construction in high-rise buildings can be easily pictured as a cabinet and its drawers [8]. With this analogy, the cabinet is the hyperstructure and the drawers are the prefabricated light-frame modular substructures. That is, a hyperstructure is a structural system that carries the loads of other complete structural systems. Hyperstructure and substructure terms are used in this article.

Two different 20-story hyperstructures were designed and modeled by using finite elements: one using glulam with external and internal bracings and another one using reinforced concrete with two internal cores. The two systems were designed in such a way that five 4-story light-frame modular substructures could be inserted. For the timber hyperstructure, glulam was preferred to CLT as an initial choice, because using the latter would have resulted in a duplication of the walls already present with the light-frame modules. The software used was RFEM [34].

The 4-story light-frame modular substructures were also modeled by using finite elements. Without a universal method to model this type of structure using finite elements, a method was developed to enable the representation of different shearwall assemblies and to obtain deflections corresponding to the empirical equations given in CSA O86-19 [35].

The structural system is completed when the substructures are inserted into the hyperstructures and then connected to the hyperfloors only or also to the columns and cores.

The studied design is a 20-story residential tower. The footprint of the building is 22 m × 28 m. The building is 60 m high, with 3 m-high stories. It has two internal shafts of 6 m × 6 m. The hyperstructure's floors (hyperfloors) were designed to be able to minimize the need for internal columns. There are two types of beams, namely the primary beams and the secondary beams. The light-frame substructures are laid on the secondary beams. The hyperfloor plan is shown in Figure 1.

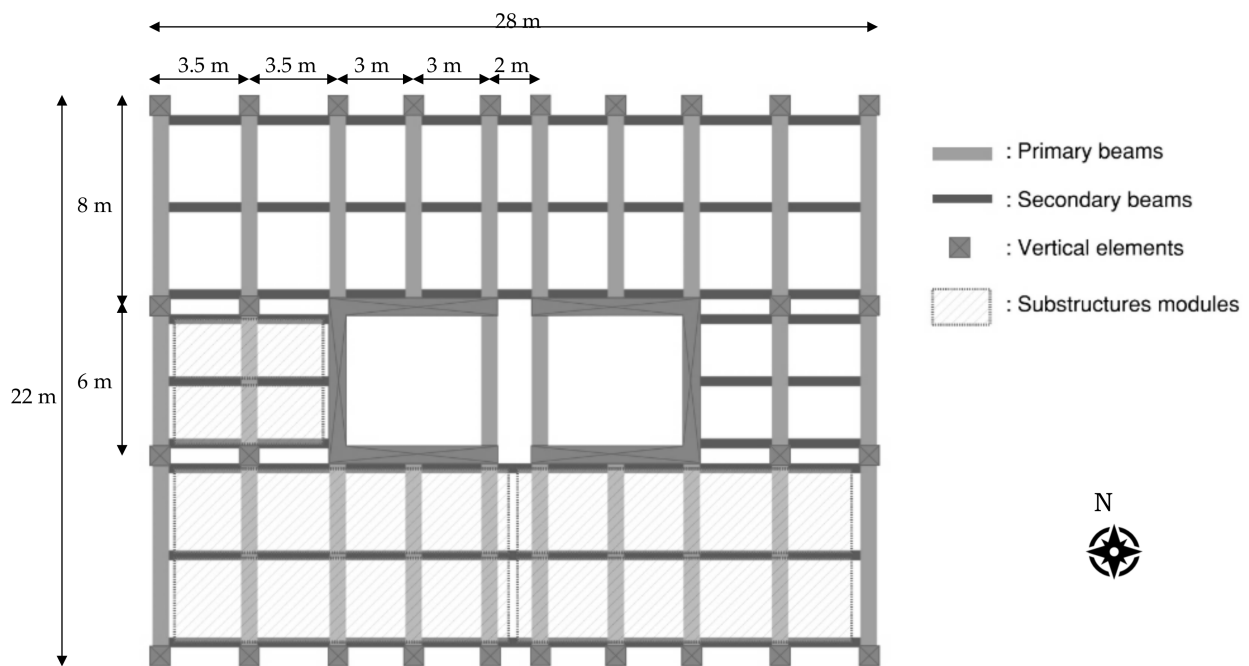


Figure 1. Hyperfloors' arrangement of beams and modules.

The vertical gravity-load-resisting system (GLRS) differs depending on the hyperstructure concept. For the glulam concept, it consists of glulam columns. For the concrete concept, it consists of concrete columns on the exterior and two concrete cores. The horizontal GLRS consists of the hyperfloors, which transfer the loads from the substructures to the vertical GLRS. For the glulam concept, they consist of glulam beams in order to keep a post-and-beam glulam system. For the concrete concept, they consist of prefabricated unidirectional concrete slabs on bidirectional concrete beams.

The LLRS differs between the concepts. For the glulam concept, the LLRS is achieved by the glulam diagonals acting as vertical trusses on the exterior walls and the service shafts. For the concrete concept, the LLRS is achieved by the two concrete cores acting as ductile shearwalls. The lateral loads are transferred through the hyperfloors by diaphragm action. For the glulam concept, the diaphragm action is achieved by steel diagonals between the glulam beams creating a horizontal truss. For the concrete concept, the diaphragm action is achieved by the concrete slabs.

For the glulam concept, the beams are assumed to be of grade SPF (spruce–pine–fir) 20f-EX and the columns and diagonals of grade SPF 14t-E. For the concrete concept, concrete with a compression strength of 30 MPa is assumed with 400 R steel rebars.

The building is assumed to be in Quebec City in the province of Quebec in Canada. Snow, wind and seismic loads are determined accordingly [36]. The design data for gravitational loads are given in Table 1, based on the NBCC.

For the hyperstructures design, modular substructures were considered as loads acting directly on the hyperfloors. Dead and live loads coming from the substructures were transformed into uniform linear loads acting on the hyperfloors' secondary beams to represent the modules' walls placed directly over them.

The design data for wind loads are given in Table 2 based on NBCC [36].

Table 1. Gravitational loads' design data according to NBCC.

Item	Value		Source Comments
Dead Load			
Self-Weight	N.A.		Managed by RFEM according to materials' densities. [37]
Roof	3.0 kPa		
Corridors	2.66 kPa		For 4-story substructures, see substructures section for details.
Floors	17.24 kPa		
Stairs	2 kPa		
Live Load			
Roof	1.0 kPa		NBCC Table 4.1.5.3.
Corridors	4.8 kPa		NBCC Table 4.1.5.3.
Floors	8.6 kPa		For 4-story substructures, see substructures section for details.
Stairs	4.8 kPa		
Snow Load			
Importance factor	ULS	1.0	NBCC Table 4.1.6.2.-A
	SLS	0.9	
Sr	0.6 kPa		NBCC Table C-2
Ss	3.6 kPa		
Roof	ULS	3.48 kPa	
	SLS	3.13 kPa	

Table 2. Wind loads' design data.

Item	Value		Source Comments
Importance Factor, I_w	ULS	1.0	NBCC Table 4.1.7.3.
	SLS	0.75	
Reference velocity pressure	q_{10}	0.41	NBCC Table C-2
	q_{50}	0.32	
Type of terrain	Rough		NBCC 4.1.7.3.5)b)
Damping ratio $\beta_{W,D}$	Glulam	0.015	NBCC 4.1.7.8.4)
	Concrete	0.020	
Average building density, ρ_B (kg/m ³)	Glulam	120	Due to the iterative process, only the final average building densities are given.
	Concrete	248	
Natural frequency in N–S axis, $f_n W$	Glulam	0.654	Due to the iterative process, only the final natural frequencies are given.
	Concrete	0.654	
Natural frequency in E–W axis, $f_n D$	Glulam	0.629	
	Concrete	0.678	

The wind loads acting on the building were calculated with the dynamic procedure following Article 4.1.7.8. of NBCC. Figure A-4.1.7.5.(2) was followed for the external pressure coefficient and the exposure factor. The effects of total and partial wind loads were considered following Figure A-4.1.7.9.(1) Apart from stress and strain caused by the wind loads, vibrations due to wind were also verified. Across- and along-wind accelerations at the top of the buildings were calculated with Equations (8) and (9) of the NBCC 2015 Commentary I [38].

Since the hyperstructure system is not well-studied and because the conditions of Article 4.1.8.7.1) of NBCC [36] are not all respected, a dynamic analysis method must be used to evaluate seismic loads and their effects. The response spectrum analysis method was used in this study. For the modal analysis, eigenvalues were extracted by the Lanczos method. To represent an adequate dynamic response, eigenvalues were extracted to have a minimum of 90% modal participating mass ratio (MPMR) in modal analysis for each orthogonal direction [38].

Once the vibration modes were extracted, the response spectrum analysis was performed. The response spectrum used is based on the 5% damped spectral response acceleration values and peak ground acceleration of Quebec City provided in table C-3 of NBCC [36]. The soil type assumed for the building was class D for stiff soil. A Lehr damping ratio of 1.5% was considered. The glulam hyperstructure's LLRS was considered as braced frames with ductile connections of limited ductility with $R_d = 1.5$ and $R_o = 1.5$. The concrete hyperstructure's LLRS was considered as ductile shear walls with $R_d = 3.5$ and $R_o = 1.6$ [36]. Respecting Article 4.1.8.12.4)b) of NBCC 2015, the effects of accidental torsional moment were accounted for. A load case was obtained for each mode of vibration, and a combination of results for all participating modes was obtained by the complete quadratic combination (CQC) method.

All elements were designed to fulfill ultimate limit state (ULS) requirements. Load effects were obtained directly from RFEM structural analysis for all load cases prescribed by NBCC. Connections were not designed in this study. All elements were also designed to fulfill serviceability limit state (SLS) requirements. A maximal deflection criterion of $L/360$ was considered as suggested in Article 9.4.3. of NBCC [36]. Apart from individual elements' deflection limits, LLRS were designed to respect interstory drift criteria: $H_s/500$ for wind loads and $H_s/40$ for seismic loads. For seismic load cases, lateral deflections were multiplied by $R_d R_o / I_E$, as prescribed in Article 4.1.8.13.2) of NBCC 2015. LLRSs were also designed so that accelerations due to wind, both along- and across-wind, were less than 15 milli-g, as prescribed by NBCC for residential buildings [37].

For the glulam hyperstructure, all connections between members were considered pinned. Reduced section properties were used for all concrete surfaces and elements according to Article 21.2.5.2 of CSA A23.3-19 [39]. The core surfaces were connected between themselves rigidly to represent traditional cast-in-place cores. Except for the cores, the concrete elements were assumed to be prefabricated. The columns were modeled with pinned connections at every four floors, resulting in prefabricated columns of 12 m. The beams and slabs in the concrete floor cassettes were assumed to be factory cast together, and rigid monolithic connections were modeled. At the intersection of the cassettes' beams with the columns and core walls, pinned connections were considered. At the interface between floor cassettes' slabs and at the interface between these slabs and the core walls, linear articulations were modeled to allow rotation along length and translation perpendicular to the intersection line. The same was performed for the roof cassettes.

The hyperstructures are shown in Figure 2.

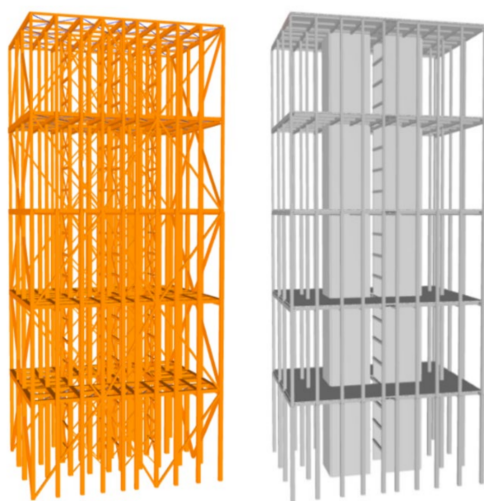


Figure 2. Axonometric view of the two designed hyperstructures without the internal substructures: glulam concept (left) and concrete concept (right).

The 5 substructures are found at levels 1–4, 5–8, 9–12, 13–16 and 17–20. The lower substructures (levels 1–4) rest directly on the foundations. The upper substructures were

at first only connected to the hyperstructure at the hyperfloors. Models were then also analyzed by connecting the modules to the columns and cores to make them participate in the LLRS.

The chosen model needed to be relatively simple and able to represent shearwalls deflections in multi-story buildings, as calculated in Article A.11.7.1 of CSA O86-19 [35]. Hence, only the substructures shearwalls and floors are modeled (Figure 3). All other elements normally composing prefabricated light-frame modules (studs, sill plates, headers, etc.) are not modeled, and the gravitational loads pass through the columns. A new model was developed based on the modified macro-element model of Chen et al. [23] in which the diagonals had hysteretic stiffnesses based on the Bouc–Wen–Baber–Noori model. For this study, the diagonals were modified as non-linear members to link with the equations of Article A.11.7.1. The concept, illustrated in Figure 4, consists of pinned frames composed of rigid beams and columns (in black). The lateral rigidity of shearwall segments is represented by diagonals with non-linear stiffnesses. Elongation of the wall anchorage system is represented with rigid connectors having linear stiffnesses in compression and tension (in blue).

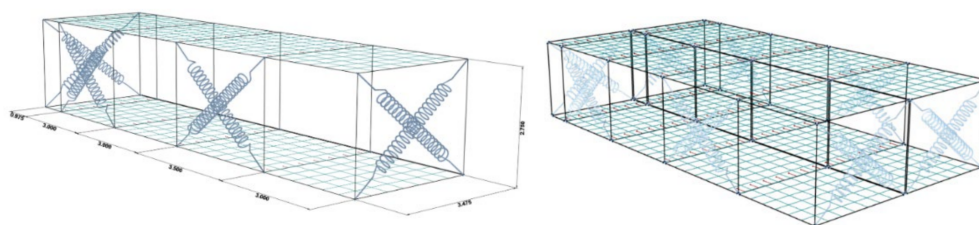


Figure 3. Modeled 3D light-frame modules.

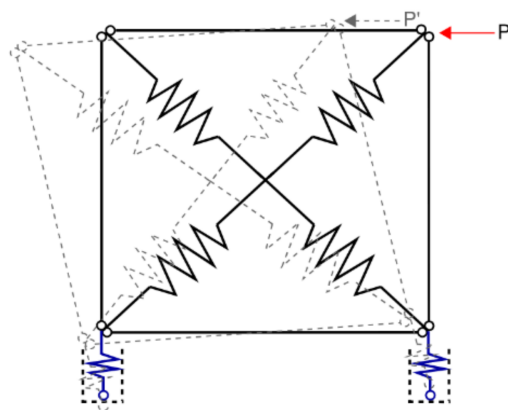


Figure 4. Shearwall segment model (adapted from [23]).

To determine the non-linear stiffness of each shearwall segment, interstory deflection due to bending, panel shear and nail slip are calculated for incremental horizontal loads of 1 kN up to the maximal shear capacity of the wall configuration. To represent the nonlinear behavior of light-frame shearwalls in the software, the deflections are calculated for 6 or 7 shear loads (e.g., for a wall with a maximal capacity of 64 kN, deflections were calculated for 1, 2, 4, 8, 20, 40 and 64 kN). Although no nonlinear analysis is conducted, modeling the substructure with non-linear diagonals allows more accurate deformations under given lateral forces.

The deflection due to vertical elongation of the wall anchorage system is taken into account by attributing axial stiffnesses in compression and in tension (using equations from Reference [40]) to the vertical connectors between modules.

Substructures' shearwalls compositions are provided in Table 3.

Table 3. Shearwall compositions used to determine the modeled stiffnesses. Note: n_{stud} is the number of members composing the end studs, n_{OSB} is the number of OSB sheets, t_{OSB} is the OSB thickness, \varnothing_{nails} is the diameter of nails and s_{nails} is the spacing between nails.

Substructures Story	End Studs		Steel Rods		Plates		Nailed Panels			
	n_{stud}	A_{stud} (mm ²)	A_{rod} (mm ²)	T_r (kN)	E_{perp} (MPa)	L_{perp} (mm)	n_{OSB}	t_{OSB} (mm)	\varnothing_{nails} (mm)	s_{nails} (mm)
4	2	10,640	307.2	85.79	517	114	1	11.0	3.05	100
3	2	10,640	307.2	85.79	517	114	2	11.0	3.05	100
2	4	21,280	307.2	85.79	517	114	2	12.0	3.05	75
1	6	31,920	307.2	85.79	517	114	2	15.0	3.33	75

The developed methodology was used to model the 3D substructures. In Figure 3, sections with springs are shearwall segments. The sections without springs are sections where there could be openings and structural or non-structural partitions. Substructure loads are presented in Table 4.

Table 4. Dead and live loads acting on the substructures' floors and roofs used in the finite element model.

Item	Value	Source Comments
Dead Load		
Roof	0.9 kPa	
Floors	1.7 kPa	Floor trusses with 38 mm light concrete screed;
Partitions	1 kPa	0.5 kPa for the seismic weight.
Mechanical, electrical and plumbing	0.5 kPa	
Walls	0.9 kPa	
Live Load		
Roof	1.0 kPa	NBCC Table 4.1.5.3
Floors	1.9 kPa	NBCC Table 4.1.5.3

In RFEM, modeling hypotheses were made. Beams and columns forming the pinned frames were modeled as highly rigid bars so that they do not deform when transferring the normal forces. All of these sections were modeled with no self-weight and with end articulations allowing rotation in the y -axis and z -axis. The frames' stability was in this way only assured by the nonlinear diagonals. Floors and ceilings were modeled as infinitely rigid surfaces hinged at each section, allowing rotation along the intersection. Vertical connections between modules were modeled as rigid bars. The top node was fixed to the floor surface. The bottom node was free to rotate along the y - and z -axes and had different axial stiffnesses in tension and compression (Table 5). Horizontal connections between modules were modeled as pinned rigid bars free to rotate along the y - and z -axes.

Table 5. Vertical connectors axial stiffnesses imported in RFEM.

Substructures Story	Axial Stiffness (kN/mm)	
	Compression	Tension
4	96.51	85.79
3	193.01	85.79
2	193.01	85.79
1	289.52	85.79

In the models with the modules participating in the LLRS, the connections between the modules and the columns were modeled with rigid bars pinned at both ends. At the column or core side, the articulation was free along the y -axis and z -axis. At the module's side,

the articulation was only free along the y -axis to prevent differential lateral displacement between the modules and the hyperstructure but to allow vertical deflection of the modules. For those models, some connections were modified to stiffen the modules and prevent substructures' modes of vibration with higher periods than the whole system's modes of vibration. The rotation along the z -axis was blocked for the horizontal connections between the modules, and pinned rigid bars were added to connect the end walls of the long modules together.

For all cases, surface loads were applied directly to the floors and roof of the modules to replace the linear loads applied to the secondary beams. Gravity-, wind- and seismic-load cases were analyzed as for the hyperstructure.

Modules' lengths are chosen so that there is a 500 mm spacing between the modules' end walls and the exterior columns. That spacing is reduced to 250 mm between the short modules' end walls and the concrete core or internal columns. A spacing of 50 mm is considered between the end walls of the long substructures.

3. Results

3.1. Comparison of Hyperstructures

To understand the impact of modular substructures on structural performance, the two hyperstructures are first analyzed and compared. The hyperstructure's cross-sections are shown in Figure 5.

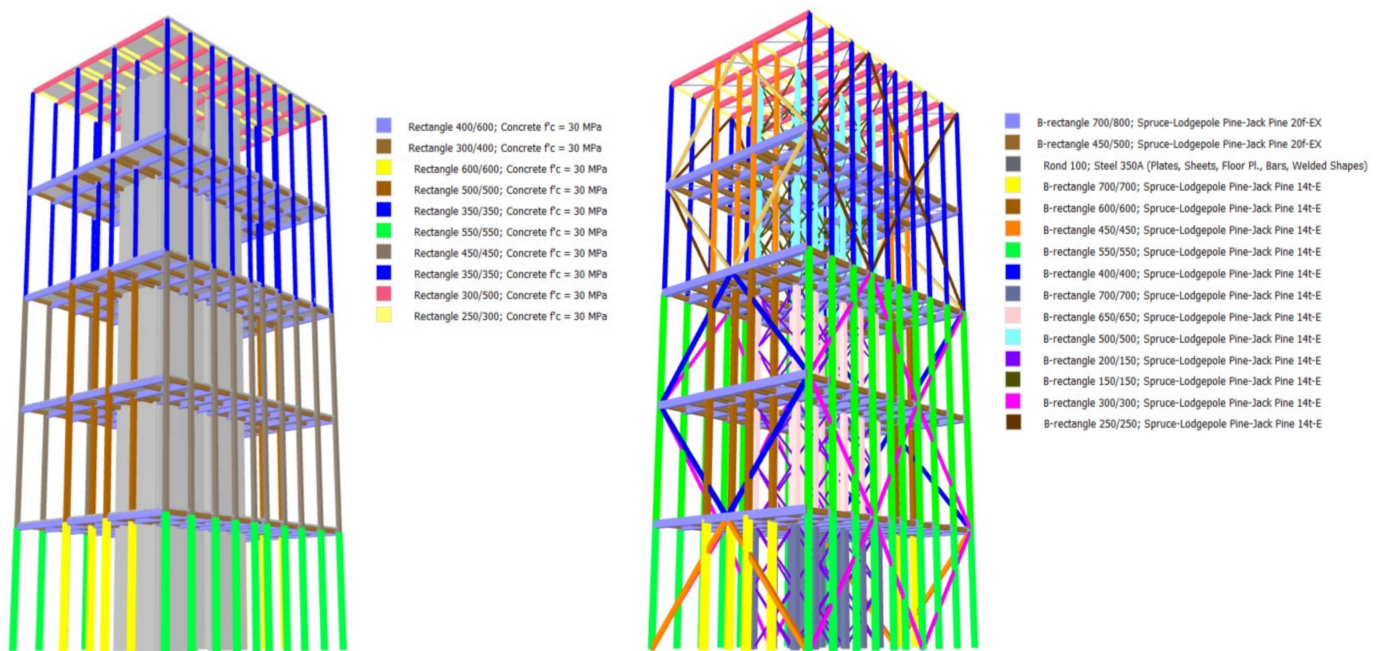


Figure 5. Hyperstructure's cross-sections: concrete (left) and glulam (right).

The self-weights of the glulam and the concrete hyperstructure were 695 and 5502 tons, respectively. Therefore, a concrete hyperstructure would require sturdier foundations than a glulam hyperstructure. The LLRS and the properties of the materials of the two hyperstructures being different, the natural frequencies vary. Table 6 shows the first natural frequencies of each hyperstructure and the MPMR associated.

For the glulam concept, the lower limit of 90% of mass participation was reached with the first two modes. For the concrete concept, the first three modes were needed to reach 90% mass participation. The final seismic base shear for the glulam and the concrete in the N–S direction was 2038 and 1867 kN, respectively. In the E–W direction, the base shear was 1975 and 1807 kN. Total deflections and interstory drifts under seismic loads are presented in Figure 6a–d. In this study, interstory drift was defined as the differential

lateral deflection between the hyperfloors. Even if the interstorey drifts varied between the concepts, the limit drift of $0.025 H_n$ was never reached. The maximum interstorey drift was 17% the limit prescribed by the NBCC.

Table 6. Periods associated with the first three modes participating in both principal axes taken from the modal analysis and modal participating mass ratio (MPMR) corresponding to the contribution of the first three modes for each concept.

Concept	N-S				E-W			
	Mode 1	Mode 2	Mode 3	MPMR	Mode 1	Mode 2	Mode 3	MPMR
Glulam	1.528	0.536	0.336	95.8%	1.591	0.567	0.340	97.8%
Concrete	1.529	0.318	0.171	91.8%	1.474	0.322	0.142	93.7%

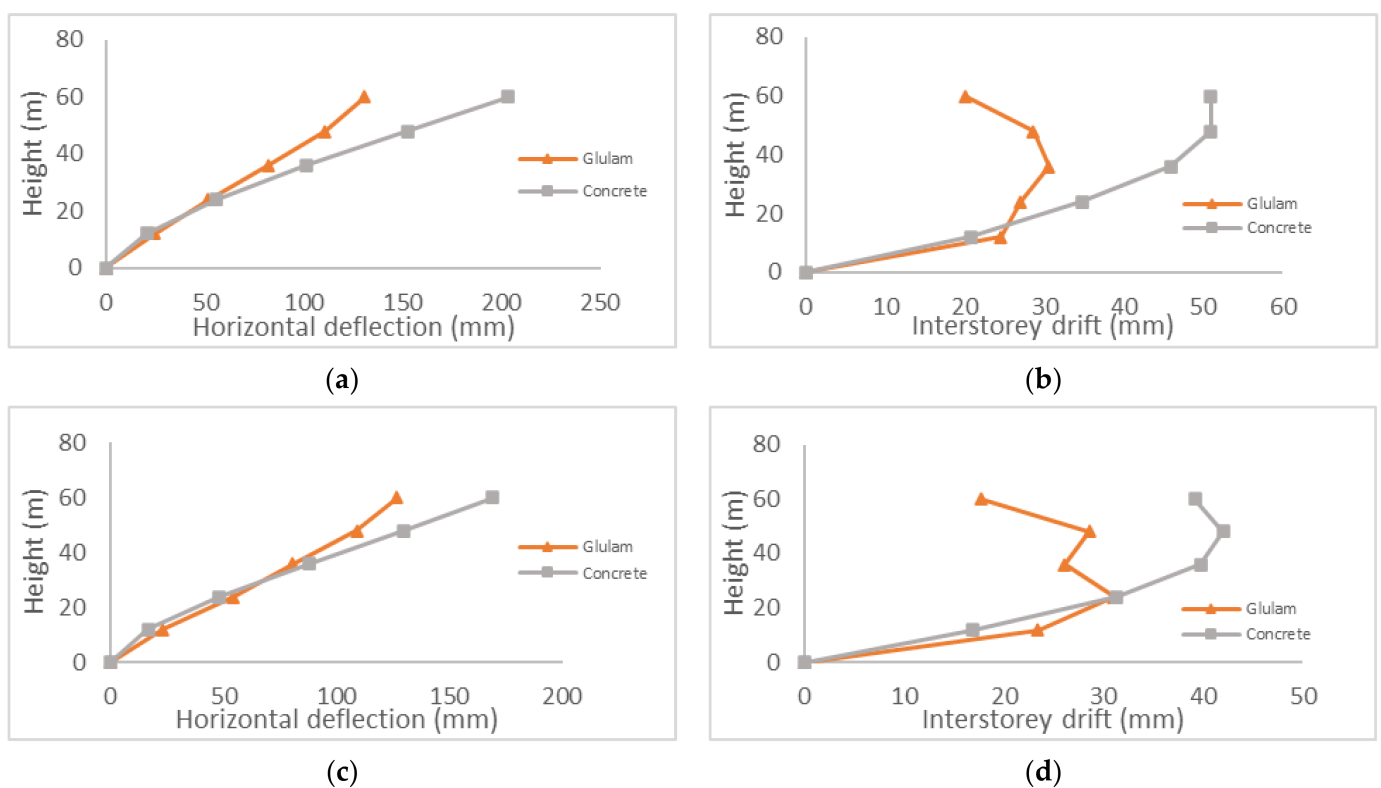


Figure 6. Total horizontal deflections ((a) N-S direction (c) E-W direction) and interstorey drifts ((b) N-S direction (d) E-W direction) associated with seismic forces.

Total deflections and interstorey drifts under wind loads are presented in Figure 7a–d. Under wind loads, the glulam hyperstructure experienced bigger deflections and drifts than the concrete hyperstructure, but the maximal interstorey drift was never higher than 25% of the limit drift ratio of $H/500$ prescribed by the NBCC.

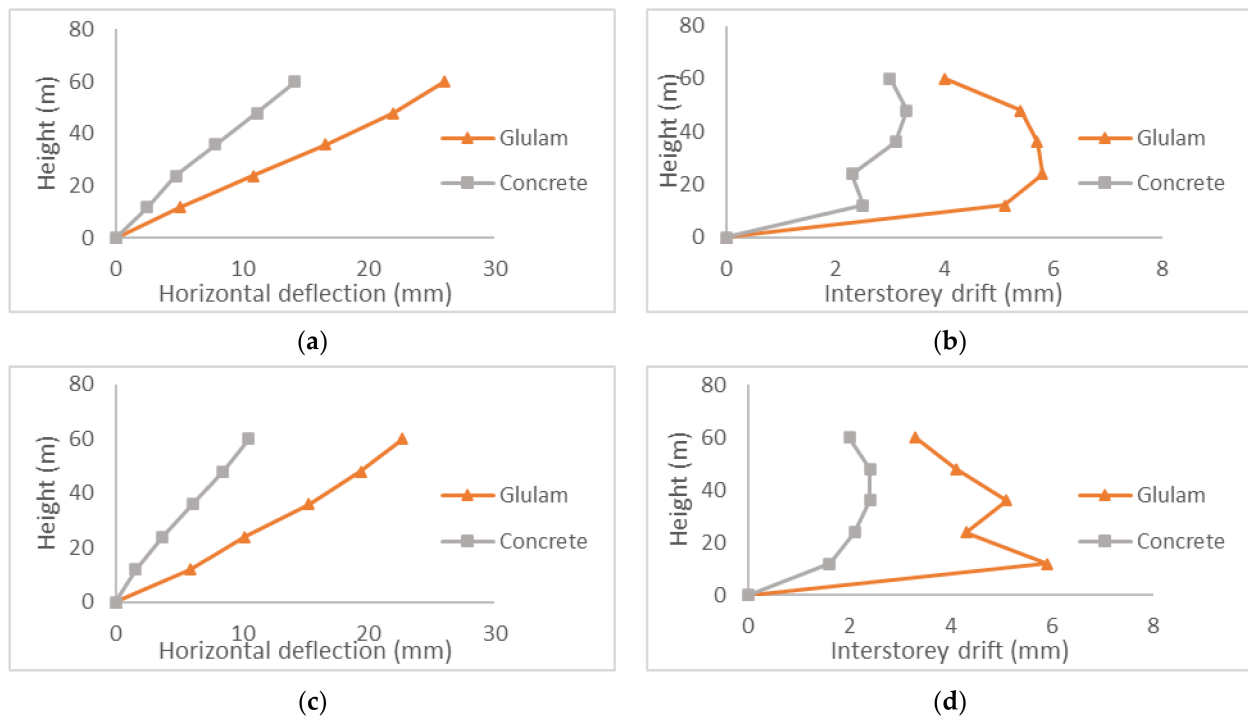


Figure 7. Total horizontal deflections ((a) N–S direction and (c) E–W direction) and interstorey drifts ((b) N–S direction (d) E–W direction) associated with wind forces.

Accelerations at the roof for both principal directions for the two concepts are presented in Table 7.

Table 7. Across- (a_w) and along-wind (a_D) accelerations at the top of the building under worst-in-10-years wind loads for both principal directions. Accelerations are expressed as a function of gravitational acceleration, g (9.81 m/s^2).

Concept	Wind N–S		Wind E–W	
	a_w	a_D	a_w	a_D
Glulam	0.48%	0.60%	0.45%	0.53%
Concrete	0.18%	0.28%	0.19%	0.25%

For both concepts, the accelerations along-wind were higher than those across-wind as would be expected since building slenderness as defined by Article 73 of Structural Commentary I [38] is higher than $1/3$. The accelerations under wind loads of all hyperstructures were below the limit for residential buildings of $1.5\% g$ [38].

3.2. Substructures Properties

The four-story substructures were analyzed, and their fundamentals periods were determined. In the N–S direction, the first mode's period was 0.545 s and in the E–W direction, it was 0.575 s . The stiffnesses of the shearwall segments at maximum capacity are shown in Table 8.

Table 8. Maximal shear capacity and lateral stiffness of the shearwall segments of the long modules.

Story	N–S 3.475 m		E–W 3.0 m		E–W 3.5 m	
	Capacity (kN)	Stiffness (kN/mm)	Capacity (kN)	Stiffness (kN/mm)	Capacity (kN)	Stiffness (kN/mm)
4	24.5	0.7	21.2	0.6	24.7	0.8
3	49.0	2.3	42.3	1.8	49.4	2.3
2	64.7	3.7	55.9	2.9	64.9	3.8
1	79.4	6.0	68.6	4.9	80.0	6.0

3.3. Integration of Substructures and Its Effect

The integration of the modeled light-frame modular substructures in the glulam and concrete hyperstructures is shown in Figure 8.

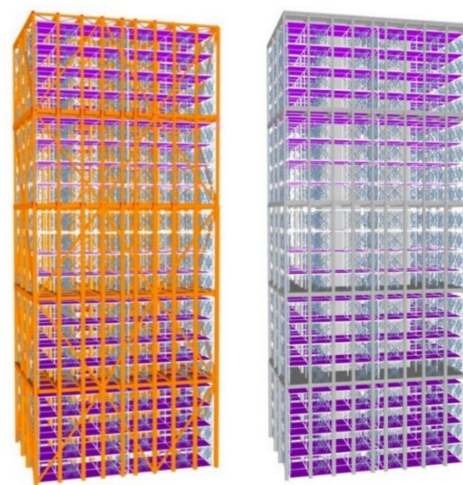


Figure 8. Glulam (left) and concrete (right) hyperstructures with the light-frame modular substructures integrated.

3.3.1. Glulam Connected to the Hyperfloors

By connecting the substructures only to the hyperfloors of the glulam concept, the minimal MPMR of 90% was reached with two modes in both directions. The first-mode shapes associated with this model and their periods are presented in Figure 9.

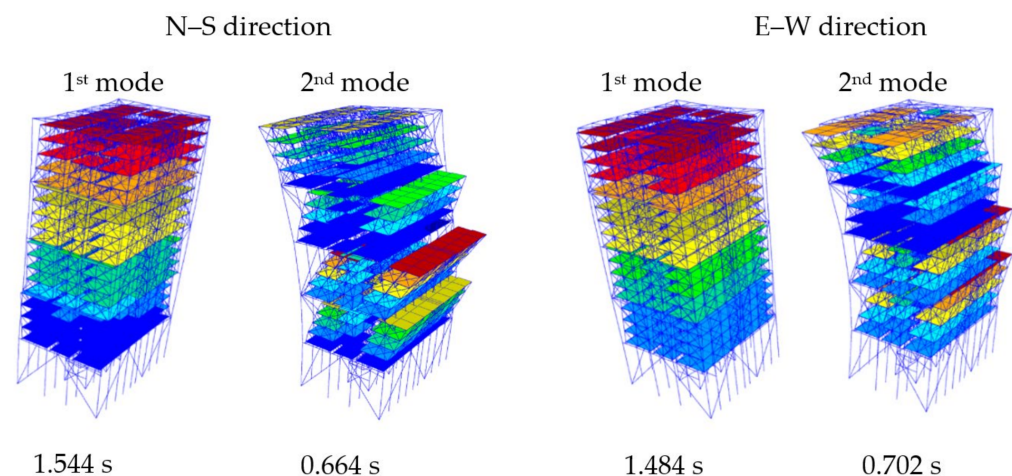


Figure 9. First mode shapes of the glulam concept with the modular substructures connected to the hyperfloors. Scale ratio of 10. Periods of the modes are under the shapes.

Compared to the hyperstructure-only model, with the substructures modeled as linear loads, fundamental periods have changed. In the N–S direction, the first mode period increased by 0.016 s (1.1%), and the second mode increased by 0.128 s (24.9%). In the E–W direction, the first mode period decreased by 0.107 s (−6.7%), and the second mode increased by 0.135 s (23.8%).

The deformation of the modules with the deflection of the beams under gravitational loads brought shear stresses to the shearwalls at the end of the modules. In day-to-day modular design, the shearwalls do not resist shear under gravitational loads. This is a particularity of this system that would need to be understood by the designers. Maximal shear forces in the end shearwalls of the modules are presented in Figure 10. Gravitational loads caused almost no shear in the shearwalls in direction E–W.

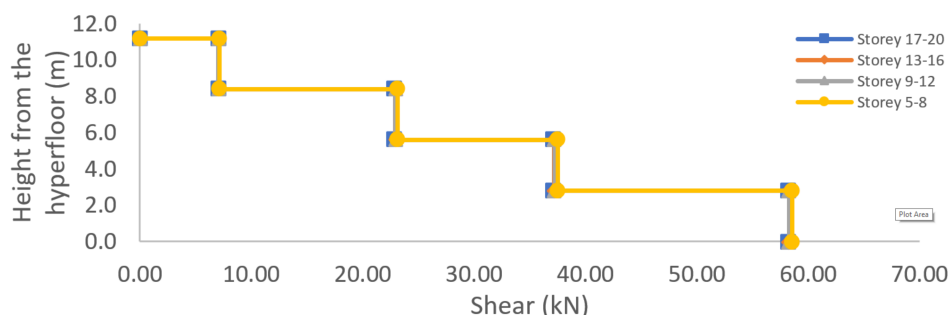


Figure 10. Shear experienced by the shearwall segments in N–S direction of the long modules under factored gravity-load combination $1.25 D + 1.5 L + 1.0 S$.

Figure 10 shows that the shear due to gravitational loads in the end shearwalls was the same for all substructures, regardless of their vertical position. The stiffer the shearwall, the more shear it experienced, as would have been expected.

Under wind loads, since the substructures were only connected to the hyperfloors, the only stresses in the shearwalls are from the deflection of the primary beams under gravity loads.

The seismic base shear in the N–S and E–W directions was 1973 and 1942 kN respectively. Figure 11 shows the shear experienced in the different shearwall segments of the long modules.

As expected under seismic forces, the higher the substructure, the higher the shear forces. For the shearwall segments of 3.0 and 3.5 m in the E–W direction that were mostly only stressed in shear under seismic loads, there could be a different design of shearwall configuration in the different substructures, with stiffer walls going up. For the shearwall segments of 3.475 m in the N–S direction, this would not be possible, since, for the shearwalls of substructures 5–8, 9–12 and 13–16, the shear induced from the deflection of the hyperfloors under gravitational loads was higher than the shear from seismic loads. For the substructures 17–20, the shear in the shearwalls under seismic loads exceeded the shear from gravitational loads by a maximum of 9.3%. Thus, for the shearwalls in the N–S direction, a uniform configuration between the substructures would be more adequate. For all substructures, the interstory drift under seismic loads was less than 40% of the limit of $0.025 H_s$ prescribed by NBCC [36].

With the modeled shearwall configurations in the N–S direction, the ratio of demand over capacity in shear was, for the 4th, 3rd, 2nd and 1st story of the substructures, 28%, 47%, 58% and 74%, respectively. With the modeled configurations in the E–W shearwalls, the maximal ratio was 8%, 19%, 24% and 29% for the shearwall of 3.0 m in length and 9%, 21%, 28% and 31% for the shearwall of 3.5 m in length. If the serviceability limits are respected and the MPMR of 90% is reachable, the shearwalls could be modified to more economical configurations.

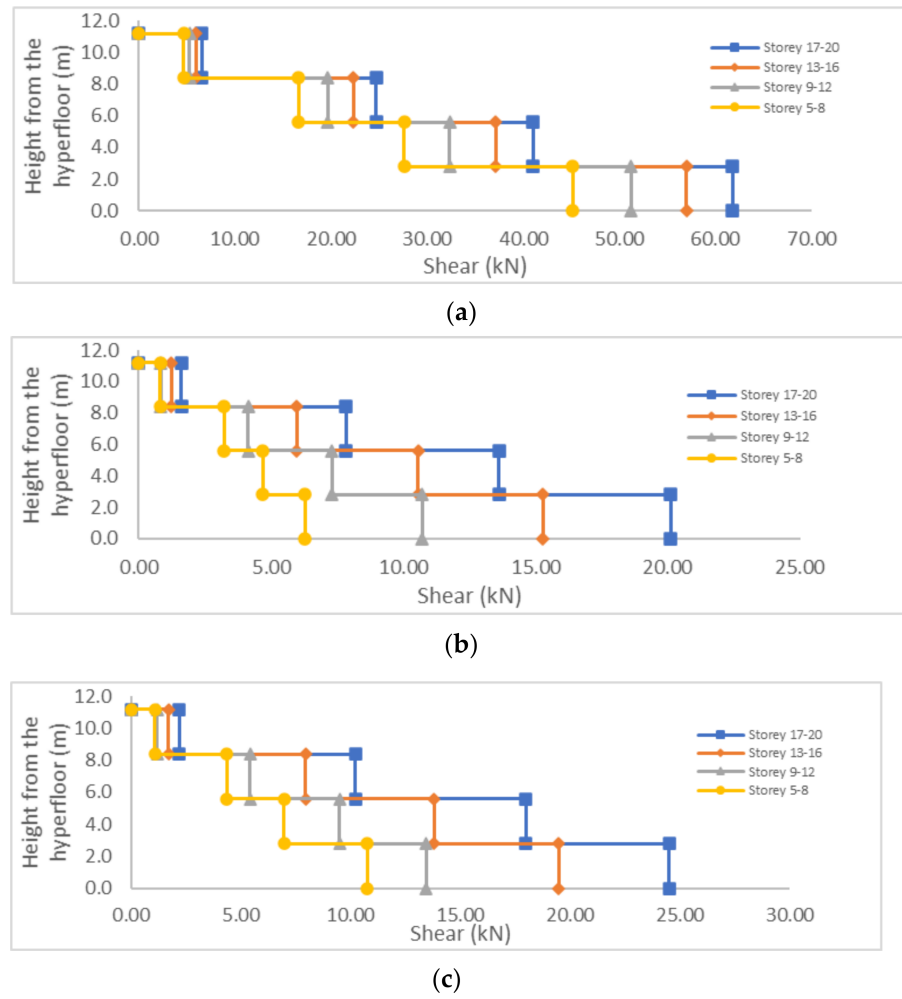


Figure 11. Shear experienced by the shearwall segments of the long modules under factored seismic-load combination $1.0 E + 1.0 D + 0.5 L + 0.25 S$. The end shearwall segments of 3.475 m in length are shown in (a), the segments of 3.0 m length are shown in (b) and the segments of 3.5 m length are shown in (c).

3.3.2. Glulam Connected to the Columns

By connecting the substructures to the hyperfloors but also to the columns of the glulam concept, the minimal MPMR of 90% was reached with three modes in both directions. The first mode shapes associated with this model and their periods are presented in Figure 12.

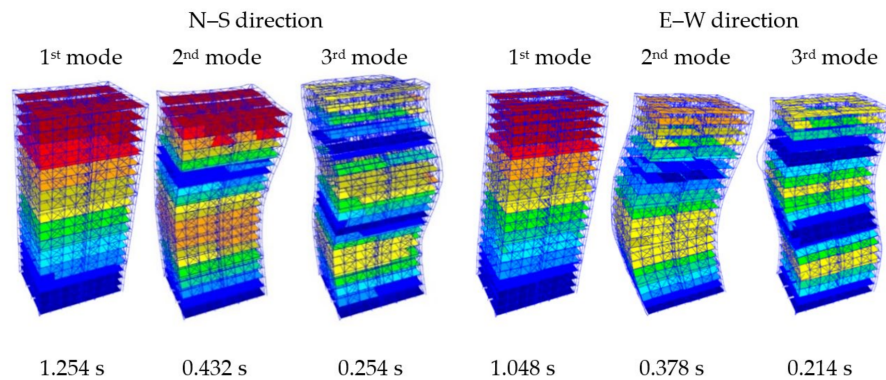


Figure 12. First mode shapes of the glulam concept with the modular substructures connected to the hyperfloors and the columns. Scale ratio of 7. Periods of the modes are under the shapes.

With the substructures participating to the LLRS, the structure was more rigid, and the periods of the modal vibrations were shorter compared to the model with the substructures only connected to the hyperfloors. In the N–S direction, the first mode period decreased by 0.290 s (−18.78%), and the second mode decreased by 0.232 s (−34.94%). In the E–W direction, the first mode period decreased by 0.436 s (−29.38%), and the second mode decreased by 0.324 s (−46.15%).

Figure 13 shows the shear experienced in the different shearwall segments of the long modules under gravity loads.

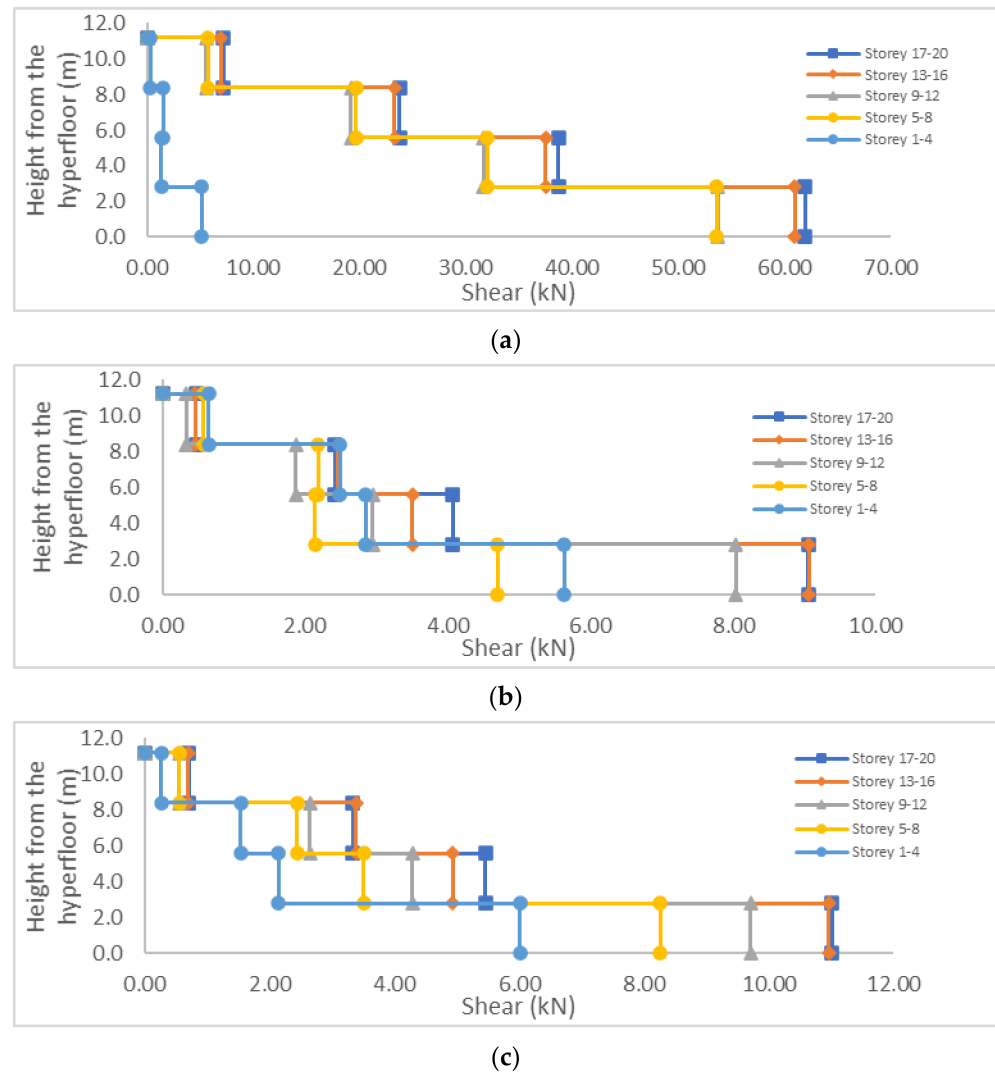


Figure 13. Shear experienced by the shearwall segments of the long modules under factored gravity-load combination $1.25 D + 1.5 L + 1.0 S$. The end shearwall segments of 3.475 m length are shown in (a), the segment of 3.0 m length are shown in (b) and the segment of 3.5 m length are shown in (c).

Figure 13 shows that, as for the model with the substructures connected only to the hyperfloors, the shearwalls in the N–S direction were much more stressed under gravitational loads than the walls in the E–W direction. On average, between the substructures, the higher ones were more stressed than the lower ones. This might be explained by the increasing with height differential vertical movement between the interior and exterior columns that caused more deflection in the higher hyperfloors and, therefore, greater deformation in the shearwalls.

With the substructures connected to the columns, the seismic loads caused more shear in the shearwalls than the wind loads. The seismic base shear was 2458 kN in the N–S

direction and 2732 kN in the E–W direction. Figure 14 shows the shear experienced in the different shearwall segments of the long modules under seismic loads.

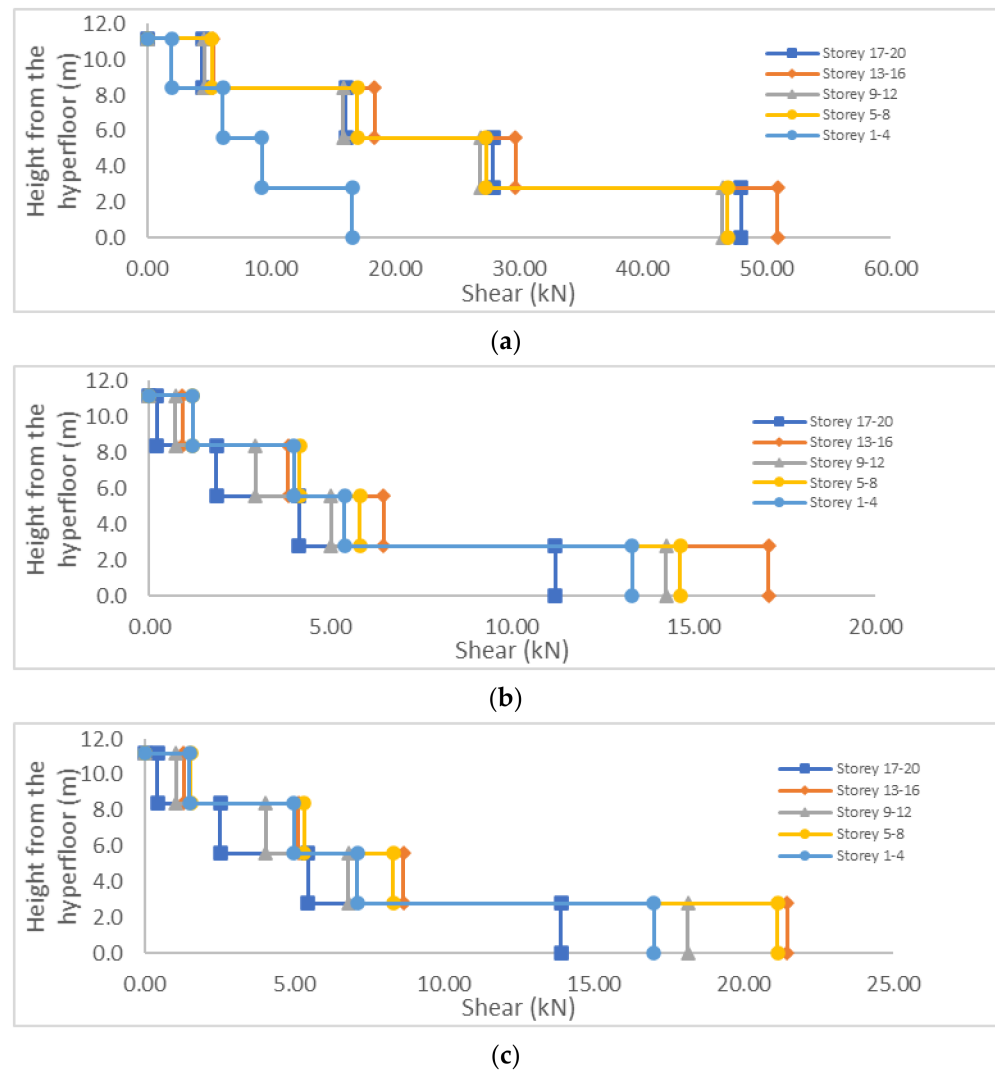


Figure 14. Shear experienced by the shearwall segments of the long modules under factored seismic-load combination $1.0 E + 1.0 D + 0.5 L + 0.25 S$. The end shearwall segments of 3.475 m length are shown in (a), the segment of 3.0 m length are shown in (b) and the segment of 3.5 m length are shown in (c).

The values of shear under seismic forces were not dependent on the vertical position of the substructure, as it was for the gravitational loads. By comparing Figures 12a and 13a, we see that the shearwalls in the N–S direction were stressed primarily by the deflection of the primary beams under gravity loads. With the modeled shearwall configurations in the N–S direction, the ratio of demand over capacity in shear was, for the 4th, 3rd, 2nd and 1st story of the substructures, of 29%, 48%, 60% and 78%, respectively. It was about the same as for the model with the substructures only connected to the hyperfloors. The gravitational-load combination governed the design of these shearwall segments.

With the same shearwall configurations in the E–W direction, the maximal ratio was 6%, 10%, 12% and 25% for the shearwall of 3.0 m in length and 6%, 11%, 13% and 27% for the shearwall of 3.5 m in length. The seismic-load combination governed the design for these shearwall segments. The ratios were about 1.1 to 2.1 times lower than they were for the model only connected to the hyperfloors. By connecting the modules to the hyperstructure, the whole system was more rigid, and, therefore, even if it caused higher

lateral seismic shear, the deflection of the system was lower, which induced less shear in the modules. If the serviceability limits are respected and the MPMR of 90% is reachable, the shearwalls could be modified to more economical configurations.

3.3.3. Concrete Connected to the Hyperfloors

By connecting the substructures only to the hyperfloors of the concrete concept, the limit of 90% for the MPMR was not reached. It was not reached, because, except for the first mode of vibration in each axis, the fundamental frequencies of the substructures were lower than the upper modes involving all the system. As can be seen in Figure 15, the upper modes of vibration were modes where the hyperstructure was still while the substructures vibrated.

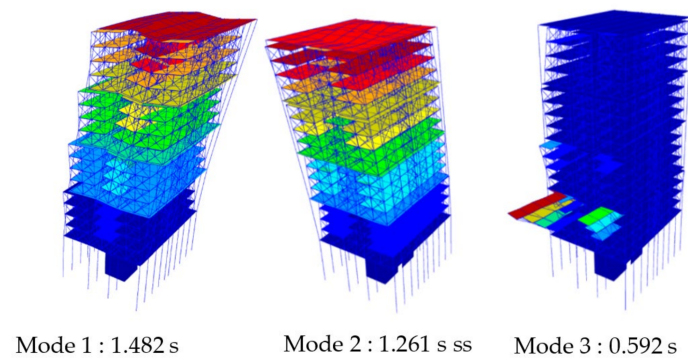


Figure 15. Vibration shapes of the first modes of the concrete hyperstructure with substructures connected only to the hyperfloors. Shapes are scaled with a ratio of 13.8. Mode 1 (left) is the first mode in the N–S direction. Mode 2 (center) is the first mode in the E–W direction. Mode 3 (right) is the next mode of vibration participating to the MPMR. The next 15 modes of vibration were only the substructures vibrate.

This was not the case for the glulam concept, because the first two modes of vibration were enough to reach the 90% MPMR, and their periods were higher than the fundamental period of the substructures, i.e., 0.545 s. Since the MPMR is not reachable, the concept, as it is, is rejected.

3.3.4. Concrete Connected to the Columns and the Cores

By connecting the substructures to the hyperfloors but also the columns and cores of the concrete concept, the minimal MPMR of 90% was reached with three modes in both directions. The first mode shapes associated with this model and their periods are presented in Figure 16.

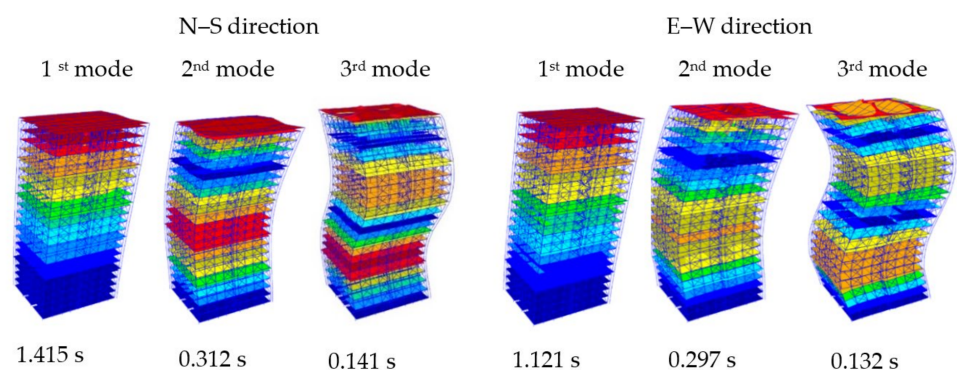


Figure 16. First mode shapes of the concrete concept with the modular substructures connected to the hyperfloors, the cores and the columns. Scale ratio of 5. Periods of the modes are under the shapes.

With the substructures participating to the LLRS, the structure was more rigid, and the periods of the modal vibrations were shorter compared to the model with the substructures modeled as linear loads. In the N–S direction, the first mode period decreased by 0.114 s (−7.5%), the second mode decreased by 0.006 s (−1.9%) and the third mode decreased by 0.030 s (−17.5%). In the E–W direction, the first mode period decreased by 0.353 s (−24.0%), the second mode decreased by 0.025 s (−7.8%) and the third mode period decreased by 0.010 s (−7.0%).

Figure 17 shows the shear experienced in the different shearwall segments of the long modules under gravity loads.

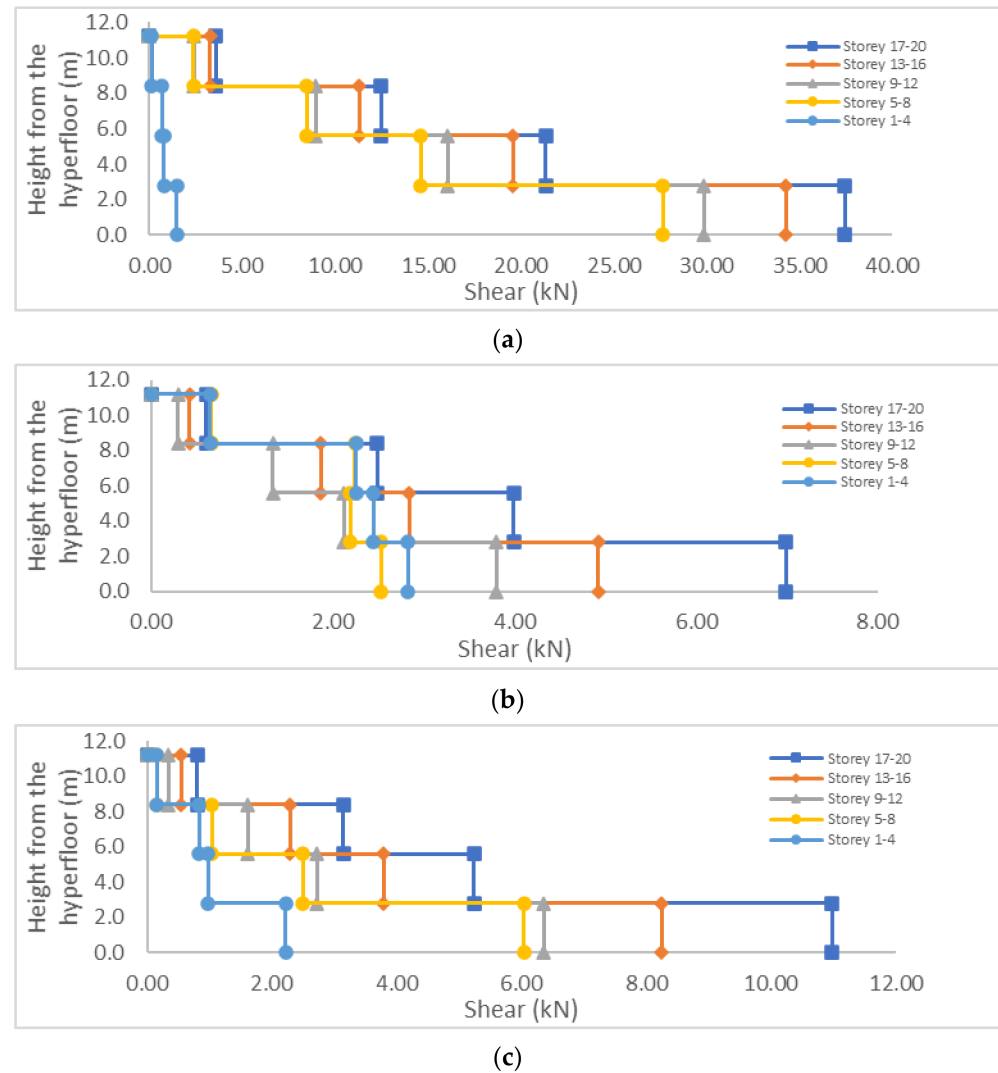


Figure 17. Shear experienced by the shearwall segments of the long modules under factored gravity-load combination $1.25 D + 1.5 L + 1.0 S$. The end shearwall segments of 3.475 m length are shown in (a), the segment of 3.0 m length are shown in (b) and the segment of 3.5 m length are shown in (c).

Figure 17 shows that, as for the glulam concept, the shearwalls in the N–S direction were much more stressed under gravitational loads than the walls in the E–W direction. On average, between the substructures, the higher ones were also more stressed than the lower ones. Compared to the glulam concept, the shear in the end shearwalls was about 1.8 times lower because the hyperfloor deflected less under the same loads.

With the substructures connected to the columns, the seismic loads caused more shear in the shearwalls than the wind loads. The seismic base shear was 2186 kN in the N–S

direction and 2243 kN in the E–W direction. Figure 18 shows the shear experienced in the different shearwall segments of the long modules under seismic loads.

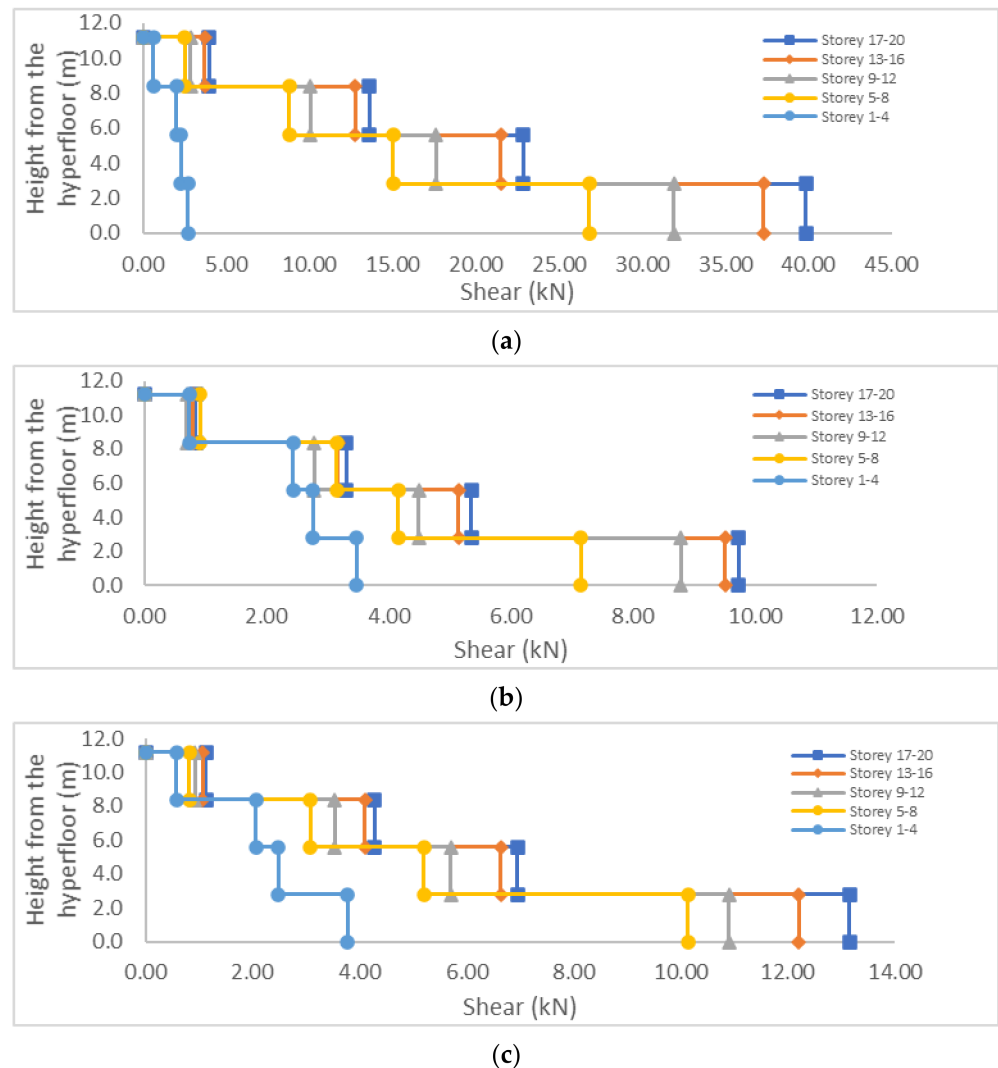


Figure 18. Shear experienced by the shearwall segments of the long modules under factored seismic-load combination $1.0 E + 1.0 D + 0.5 L + 0.25 S$. The end shearwall segments of 3.475 m length are shown in (a), the segment of 3.0 m length are shown in (b) and the segment of 3.5 m length are shown in (c).

As for the gravitational loads, the higher substructures were more stressed than the lower ones. With actual modeled shearwalls configurations in the N–S direction, the ratio of demand over capacity in shear was, for the 4th, 3rd, 2nd and 1st story of the substructures, 14%, 25%, 33% and 47%, respectively. The gravitational-load combination governed the design of these shearwalls segments. With the same shearwall configurations in the E–W direction, the maximal ratio was 4%, 8%, 10% and 14% for the shearwall of 3.0 m length and 5%, 9%, 11% and 16% for the shearwall of 3.5 m length. As for the glulam concept, the seismic-load combination governed the design for these shearwalls segments, but the ratios were a little lower. If the serviceability limits are respected and the MPMR of 90% is reachable, the shearwalls could be modified to more economical configurations.

4. Conclusions

This finite element study explored some structural aspects of an innovative way of using prefabricated light-frame modular construction in high-rise buildings. Aspects such

as fire resistance or floor vibrations, which have not been studied in this project, should be investigated to make this structural system more compliant with the prescribed standards and legal documentation.

In this study, a glulam and a concrete hyperstructure were developed and designed for a 20-story building, and a method was developed to model the modular light-frame substructures that are part of the system. The interaction between the two systems and the impact of and on the substructures were analyzed, and the following conclusions can be derived:

- The glulam hyperstructure concept for a 20-story building is viable for both the modular substructures connected only to the hyperfloors and the modular substructures connected to the columns and the hyperfloors.
- The concrete hyperstructure concept for a 20-story building is viable only if the modular substructures are connected to the columns, the cores and the hyperfloors.
- Conventional configurations of shearwalls are sufficient to resist the shear from the gravitational, wind and seismic loads.
- In contrast to other structural systems, gravitational forces can induce significant shear in the modules' shearwalls.

Hyperstructure systems could contribute to the use of light-frame structures above six stories. This structural system could increase the speed of erection, improve the quality of components and installation work, decrease construction costs and further increase the use of timber in residential high-rise buildings.

More research needs to be performed on this type of structural system. For example, the design of the connections between the modular substructures and the hyperstructure is of primary importance and should be investigated, and the required space between the substructures and the hyperstructure should be determined. To understand the dynamic properties of such buildings, the implementation of a hysteretic light-frame shearwalls model would be necessary.

Author Contributions: Conceptualization, N.L., S.M. and P.B.; methodology, N.L.; software, N.L.; validation, N.L., S.M., M.O. and P.B.; formal analysis, N.L.; investigation, N.L.; data curation, N.L.; writing—original draft preparation, N.L.; writing—review and editing, N.L., P.B., S.M. and M.O.; supervision, S.M., M.O. and P.B.; project administration, P.B.; funding acquisition, P.B. All authors have read and agreed to the published version of the manuscript.

Funding: The authors are grateful to Natural Sciences and Engineering Research Council of Canada for the financial support through its IRC and CRD programs (IRCPJ 461745-18 and RDCPJ 514294-17), as well as the industrial partners of the NSERC industrial chair on eco-responsible wood construction (CIRCERB), the industrial partners of the industrialized construction initiative (ICI) and the Créneau Accord Bois Chaudière-Appalaches (BOCA).

Data Availability Statement: The models presented in this study are openly available at this link: <https://www.researchgate.net/project/Finite-Element-Study-of-Hyperstructure-Systems-with-Modular-Light-Frame-Construction-in-High-Rise-Buildings> (accessed on 7 January 2022).

Conflicts of Interest: The authors declare no conflict of interest. The funders had no role in the design of the study; in the collection, analyses or interpretation of data; in the writing of the manuscript; or in the decision to publish the results.

References

1. United Nations Department of Economic and Social Affairs Population Division. *World Urbanization Prospects: The 2018 Revision*; United Nations Publications: New York, NY, USA, 2019.
2. Ali, M.M.; Armstrong, P.J. Overview of Sustainable Design Factors in High-Rise Buildings. In *CTBUH 2008, 8th World Congress-Tall and Green: Typology for a Sustainable Urban Future, Congress Proceedings*; Council on Tall Buildings and Urban Habitat: Dubai, United Arab Emirates, 2008; pp. 282–291. [[CrossRef](#)]
3. Skidmore Owings and Merrill LLP. *Timber Tower Research Project*; SOM: Chicago, IL, USA, 2013.
4. Smith, R.E. *Prefab Architecture: A Guide to Modular Design and Construction*; John Wiley & Sons: Hoboken, NJ, USA, 2011. [[CrossRef](#)]

5. Bertram, N.; Fuchs, S.; Mischke, J.; Palter, R.; Strube, G.; Woetzel, J. *Modular Construction: From Projects to Products*; McKinsey & Company: Atlanta, GA, USA, 2019. [CrossRef]
6. Pan, Y.; Tannert, T.; Kaushik, K.; Xiong, H.; Ventura, C.E. Seismic Performance of a Proposed Wood-Concrete Hybrid System for High-Rise Buildings. *Eng. Struct.* **2021**, *238*, 112194. [CrossRef]
7. Bjertnaes, M.A.; Malo, K.A. Wind-Induced Motions of TREET. In Proceedings of the World Conference on Timber Engineering (WCTE 2014), Quebec City, QC, Canada, 10–14 August 2014.
8. Malo, K.A.; Abrahamsen, R.B.; Bjertnæs, M.A. Some Structural Design Issues of the 14-Storey Timber Framed Building "Treet" in Norway. *Eur. J. Wood Wood Prod.* **2016**, *74*, 407–424. [CrossRef]
9. Utne, I. Numerical Models for Dynamic Properties of a 14 Storey Timber Building. Master's Thesis, Norwegian University of Science and Technology, Trondheim, Norway, 2012.
10. Abrahamsen, R.B.; Malo, K.A. Structural Design and Assembly of "Treet"-A 14-Storey Timber Residential Building in Norway. In Proceedings of the World Conference on Timber Engineering (WCTE 2014), Quebec City, QC, Canada, 10–14 August 2014.
11. Kaushik, K. Feasibility Study of Tall Concrete-Timber Hybrid System. Master's Thesis, University of British Columbia, Vancouver, BC, Canada, 2017. [CrossRef]
12. Chen, J.; Xiong, H.; Ventura, C.E. Non-Linear Simplified Models for Seismic Response Estimation of a Novel Tall Timber-Concrete Hybrid Structural System. *Eng. Struct.* **2021**, *229*, 111635. [CrossRef]
13. Xiong, H.; Chen, J.; Wu, Y. Research on Seismic Performance of a Concrete-Wood Hybrid Structural System for Tall Building. *J. Build Struct.* **2018**, *39*, 62–70.
14. Xiong, H.; Ouyang, L.; Wu, Y.; Lu, S. Preliminary Design of a Novel Hybrid Tall Building with Concrete Frame-Tube and Light-Wood Boxes. In Proceedings of the World Conference on Timber Engineering, Vienna, Austria, 22–25 August 2016.
15. Abrahamsen, R. Mjøstårnet-Construction of an 81 m Tall Timber Building. In Proceedings of the Internationales Holzbau-Forum IHF 2017, Garmisch-Partenkirchen, Germany, 6–8 December 2017.
16. de Jong, R. Tall Timber Buildings. Master's Thesis, Eindhoven University of Technology, Eindhoven, The Netherlands, 2017.
17. Connolly, T.; Loss, C.; Iqbal, A.; Tannert, T. Feasibility Study of Mass-Timber Cores for the UBC Tall Wood Building. *Buildings* **2018**, *8*, 98. [CrossRef]
18. NEWBuildS. Application of Analysis Tools from NEWBuildS Research Network in Design of a High-Rise Wood Building. 2013. Available online: <https://www.bcfii.ca/wp-content/uploads/2021/02/fii415-2014-15-newbuilds-application-of-analysis-tools-in-design-of-high-rise-wood-building-1.pdf> (accessed on 7 January 2022).
19. Lawson, R.M.; Ogden, R.G.; Bergin, R. Application of Modular Construction in High-Rise Buildings. *J. Archit. Eng.* **2012**, *18*, 148–154. [CrossRef]
20. Gardiner, P. The Construction of a High-Rise Development Using Volumetric Modular Methodology. In *The Future of Tall: A Selection of Written Works on Current Skyscraper Innovations*; CTBUH: Chicago, IL, USA, 2015; pp. 136–143.
21. Hickory. Hickory Building Systems. Overview of Prefabricated Structural System. Available online: <https://www.hickory.com.au/wp-content/uploads/2021/11/hickory-building-systems-overview.pdf> (accessed on 7 January 2022).
22. Van de Kuilen, J.-W. Hotel Jakarta Amsterdam an 8 Storey Hotel with 3D Modules. In Proceedings of the Woodrise 2019, Québec, QC, Canada, 2 October 2019.
23. Chen, Z.; Chui, Y.H.; Doudak, G.; Ni, C.; Mohammad, M. Simulation of the Lateral Drift of Multi-Storey Light Wood Frame Buildings Based on a Modified Macro-Element Model. In Proceedings of the World Conference on Timber Engineering (WCTE 2014), Quebec City, QC, Canada, 10–14 August 2014.
24. Chen, Z.; Chui, Y.H.; Chun, N.; Xu, J. Seismic Response of Midrise Light Wood-Frame Buildings with Portal Frames. *J. Struct. Eng.* **2013**, *140*, A4013003. [CrossRef]
25. Casagrande, D.; Rossi, S.; Sartori, T.; Tomasi, R. Proposal of an Analytical Procedure and a Simplified Numerical Model for Elastic Response of Single-Storey Timber Shear-Walls. *Constr. Build. Mater.* **2015**, *102*, 1101–1112. [CrossRef]
26. Malesza, J. Effective Model for Analysis of Wood-Framed Timber Structures. *Arch. Civ. Eng.* **2017**, *63*, 99–112. [CrossRef]
27. Ormarsson, S.; Vessby, J.; Johansson, M.; Kua, L. Numerical and Experimental Study on Modular-Based Timber Structures. In Proceedings of the 2019 Modular and Offsite Construction (MOC) Summit, Banff, AB, Canada, 21–24 May 2019; pp. 471–478. [CrossRef]
28. Togay, A.; Anil, Ö.; Karagöz İşleyen, Ü.; Ediz, İ.; Durucan, C. Finite-Element Analyses of Light Timber-Framed Walls with and without Openings. *Proc. Inst. Civ. Eng. Struct. Build.* **2017**, *170*, 555–569. [CrossRef]
29. Cárcamo, S.; María, H.S.; Zisis, S. Wood Frame Shear Wall Model for a Finite Element Program through a Shell Element. In Proceedings of the WCTE 2018-World Conference on Timber Engineering, Seoul, Korea, 20–23 August 2018.
30. Tarabia, A.M.; Itani, R.Y. Static and Dynamic Modeling of Light-Frame Wood Buildings. *Comput. Struct.* **1997**, *63*, 319–334. [CrossRef]
31. Folz, B.; Filiatrault, A. Simplified Seismic Analysis of Woodframe Structures. In Proceedings of the 13th World Conference on Earthquake Engineering, Vancouver, BC, Canada, 1–6 August 2004.
32. Collins, M.; Kasal, B.; Paevere, P.; Foliente, G.C. Three-Dimensional Model of Light Frame Wood Buildings. I: Model Description. *J. Struct. Eng.* **2005**, *131*, 676–683. [CrossRef]
33. Xu, J.; Dolan, J.D. Development of a Wood-Frame Shear Wall Model in ABAQUS. *J. Struct. Eng.* **2009**, *135*, 977–984. [CrossRef]
34. *Dlubal Software GmbH, RFEM Version 5.25*; Structural Engineering Software for Analysis and Design: Tiefenbach, Germany, 2021.

35. CSA O86-19; Engineering Design in Wood. CSA Group: Toronto, ON, Canada, 2019.
36. National Research Council of Canada; Canadian Commission on Building and Fire Codes. *National Building Code of Canada 2015*; National Research Council of Canada: Ottawa, ON, Canada, 2015. [[CrossRef](#)]
37. Bezabeh, M.A.; Bitsuamlak, G.T.; Popovski, M.; Tesfamariam, S. Dynamic Response of Tall Mass-Timber Buildings to Wind Excitation. *J. Struct. Eng.* **2020**, *146*, 5–6. [[CrossRef](#)]
38. National Research Council of Canada; Canadian Commission on Building and Fire Codes; Standing Committee on Structural Design; Standing Committee on Earthquake Design. *Structural Commentaries (User's Guide: NBC 2015: Part 4 of Division B)*; National Research Council of Canada: Ottawa, ON, Canada, 2017. [[CrossRef](#)]
39. CSA A23.3-19; Design of Concrete Structures. CSA Group: Toronto, ON, Canada, 2019.
40. Newfield, G.; Ni, C.; Wang, J. *Design Example: Design of Stacked Multi-Storey Wood-Based Shear Walls Using a Mechanics-Based Approach*; FPInnovations: Pointe-Claire, QC, Canada; Canadian Wood Council: Ottawa, ON, Canada, 2013.